Electronic Supplementary Material (ESI) for Nanoscale.

Supplementary information for

High performance graphene/few-layer InSe photo-detector

Zhesheng Chen, [a,b] Johan Biscaras,[a] and Abhay Shukla *[a]

[a] Institut de Minéralogie, de Physique des Matériaux, et de Cosmochimie (IMPMC), Sorbonne Universités - UPMC Univ Paris 06, UMR CNRS 7590, MNHN, IRD UMR 206, 4 Place Jussieu, F-75005 Paris, France.

[b] School of Nuclear Science and Technology, Lanzhou University, Lanzhou 730000, PR China.

Corresponding Author

*Email: abhay.shukla@impmc.upmc.fr.

1. Fabrication process of photo-detector based on graphene/InSe heterostructure

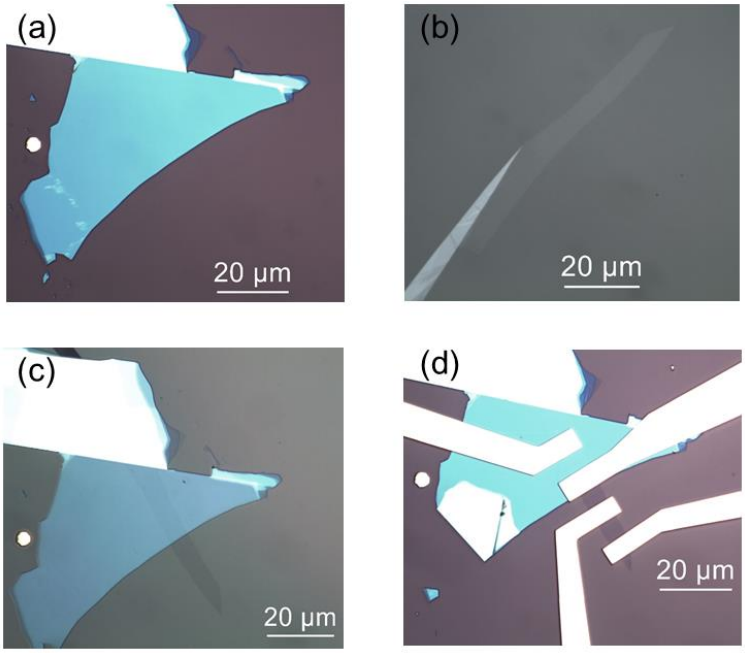

Figure S1. Fabrication process of Graphene/20-layer InSe heterostructure. (a) 20-layer InSe prepared on SiO_2/Si by mechanical exfoliation method. (b) Monolayer graphene prepared on glass using anodic bonding method. (c) Monolayer graphene transferred on top of 20-layer InSe. (d) Cr/Au electrodes fabricated by electron beam lithography and evaporation.

2. Characterization and measurement of graphene/few-layer InSe photo-detector

The crystal structure of few-layer InSe was characterized by field emission transmission electron microscopy (TEM JEOL 2100F) with the electron energy at 200 keV. The vibrational properties of few-layer InSe were analyzed using a Horiba Jobin-Yvon Xplora Raman spectrometer in a back scattering geometry under ambient conditions and with 532 nm and 638 nm wavelength laser light.

To avoid heating with the focused spot of 1µm laser power of 12 µW was used. To characterize photo-detection, the whole device was illuminated by the 532 nm laser using different illumination powers and the electrical data were recorded with Keithley 2400 multimeters.

3. Degradation of 20-layer InSe in ambient conditions

We characterized the stability of 20-layer InSe (used in our device) by Raman spectroscopy in ambient conditions over a longer 2 month period as shown in figure S3. The Raman intensity of InSe decreases by more than one-third which means that even for the 20-layer sample, the top 7~8 layers are degraded over time. Thus even here, the graphene encapsulation ensures the integrity of the device.

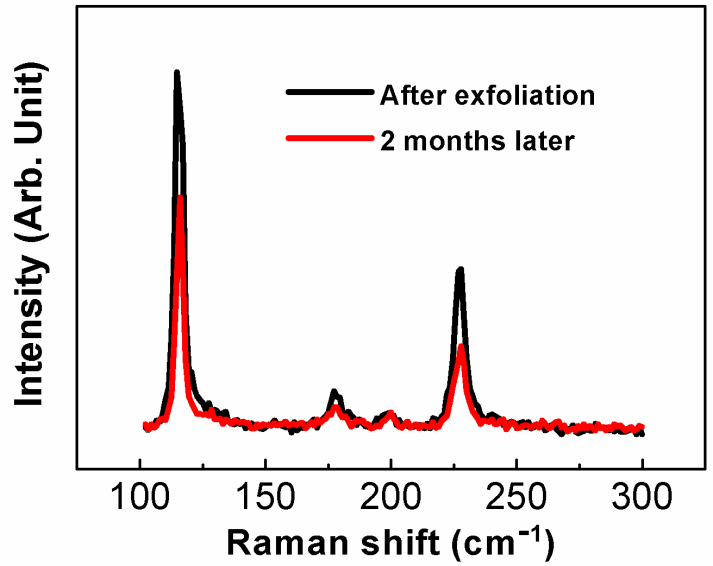

Figure S2. Raman characterization of 20-layer InSe after exfoliation and 2 months later in ambient conditions.

4. Raman shift of graphene

From the Raman shift of G and 2D vibration modes, one can estimate the quality and the doping level of graphene.[S1,S2] In our experiment, we compare the graphene made by mechanical exfoliation method, the graphene prepared by anodic bonding method and the wedging transferred graphene on SiO_2/Si substrate. For the graphene made by mechanical exfoliation, the G mode is at 1581.5 cm^{-1} and 2D mode is at 2670.8 cm^{-1}.[S3] For the graphene prepared by anodic bonding method, no defect peaks are observed and the two modes both have a clear blue shift, at 1598.8 cm^{-1} and 2678.1 cm^{-1} indicating hole doping.[S4] For the transferred anodic bonded graphene, the Raman peaks are at 1587.5 cm^{-1} and 2685.1 cm^{-1} for G and 2D modes respectively, which again shows hole doping compared with mechanically exfoliated graphene. This hole doping can result from wedging transfer or water vapor[S5,S6] and is confirmed by the I_{ds}-V_g characterization of the graphene/20-layer InSe heterosturcture in which the Dirac point is at 20 V.

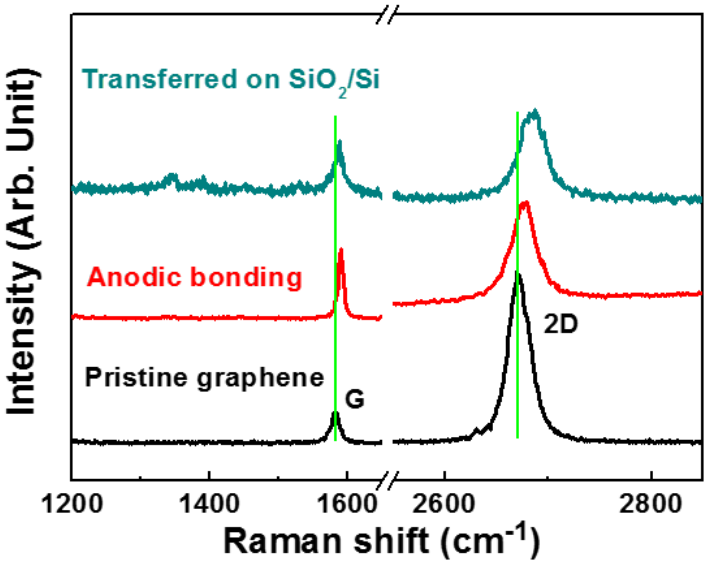

Figure S3. Raman shift of graphene prepared by mechanical exfoliation method (pristine graphene), graphene prepared by anodic bonding method and the anodic bonded graphene transferred on SiO_2/Si. The green lines indicate the positions of G and 2D vibration modes in pristine graphene.

5. Homostructural Photo-detector based on few-layer InSe

Mechanically exfoliated 20-layer InSe is used for fabricating a photo-detector whose photocurrent is characterized by applying source-drain voltage and back gate voltage respectively. During the photocurrent measurement, the whole device is illuminated by the laser at the wavelength of 532 nm. The photocurrent is measured under different illumination power as a function of source-drain voltage. In addition, the photocurrent as a function of back gate voltage is also characterized under the illumination power of 12.6 W/m^2. The photocurrent is of order of magnitude ~ nA even with V_{ds}=5 V and various back gate voltages. The photoresponsivity (R) and external quantum efficiency (EQE) can be finally calculated by taking into account the effective area of the device which is 35.2 μm^2 (the effective area of the heterostructure is 30.8 μm^2).

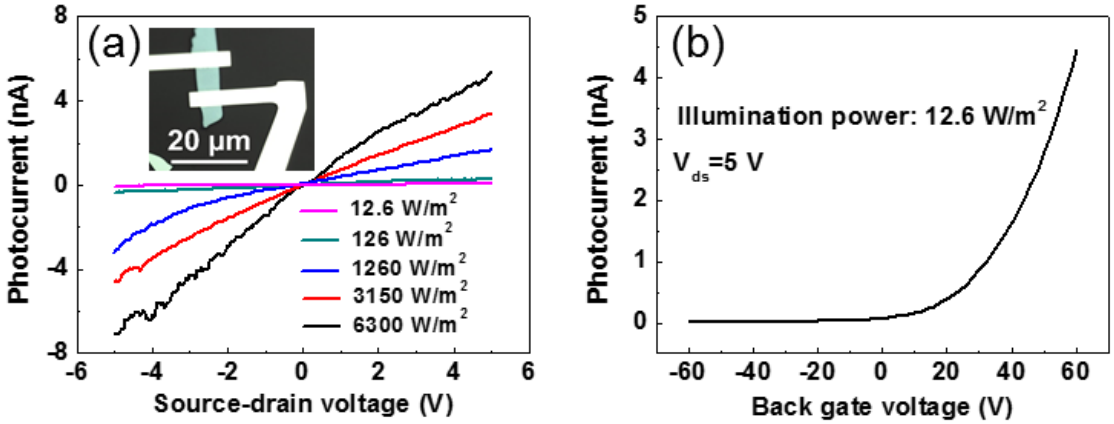

Figure S4. (a) Power dependent photocurrent as a function of source drain voltage at V_g=0 V. Insert: optical image of 20-layer InSe. (b) Photocurrent as a function of back gate voltage at V_{ds}=5 V.

6. Schematics of photo-detector based on few-layer InSe and graphene/few-layer InSe heterostructure

In InSe single crystal, the values of mean carrier mean free path are 1.75 nm and 5.08 nm in the directions parallel and perpendicular to the c-axis respectively.[S7] This means that in our few-layer InSe device (shown in figure S4 (a)), the effective junction volume where the photoexcited electrons can flow into the drain contact before recombination (defined by the mean free paths and the drain/InSe interface) is 5.3×10^{-5} μm^3. However in the graphene/InSe heterostructure (shown in figure S1 (d)), the effective junction area is the the whole graphene covered surface of the device. The effective junction volume is 5.4×10^{-2} μm^3 which is more than 10^3 times larger than in few-layer InSe. This situation is schematized in figure S5.

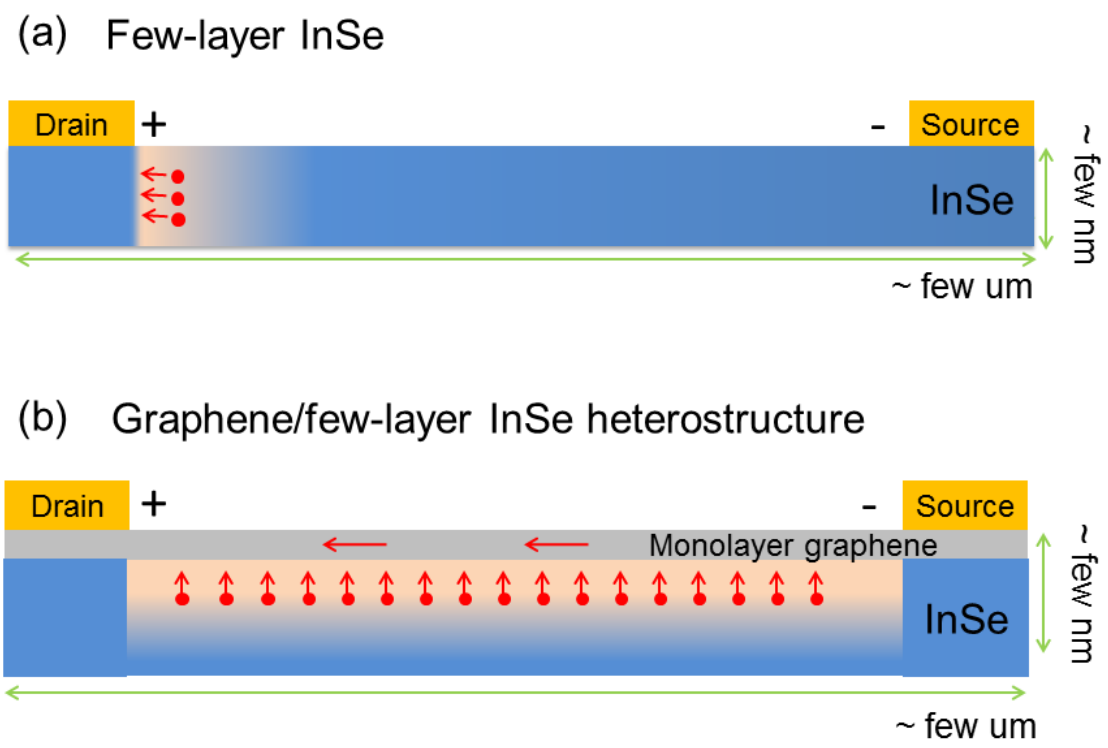

Figure S5. (a) Schematics of photo-detector based on few-layer InSe. (b) Schematics of photo-detector based on graphene/few-layer InSe heterostructure. The highlighted pink region demarcates the effective volume in the devices from which charge carriers can be extracted. The full red circles represent photo-excited electrons.

References

S1 M. Bruna, A. K. Ott, M. Ijäs, D. Yoon, U. Sassi and A. C. Ferrari, 2014, arXiv:1405.4264v1.

S2 A. Tiberj, M. Rubio-Roy, M. Paillet, J.-R. Huntzinger, P. Landois, M. Mikolasek, S. Contreras, J.-L. Sauvajol, E. Dujardin and A.-A. Zahab, *Sci. Rep.*, 2013, **3**, 2355.

S3 S. Berciaud, S. Ryu, L. E. Brus and T. F. Heinz, *Nano Lett.*, 2009, **9**, 346–352.

S4 T. Moldt, A. Eckmann, P. Klar, S. V. Morozov, A. A. Zhukov, K. S. Novoselov and C. Casiraghi, *ACS Nano*, 2011, **5**, 7700–7706.

S5 J. Shim, C. H. Lui, T. Y. Ko, Y.-J. Yu, P. Kim, T. F. Heinz and S. Ryu, *Nano Lett.*, 2012, 12, 648–654.

S6 W. Zhang, C. P. Chuu, J. K. Huang, C. H. Chen, M. L. Tsai, Y. H. Chang, C. T. Liang, Y. Z. Chen, Y. L. Chueh, J. H. He, M. Y. Chou and L. J. Li, *Sci. Rep.*, 2014, **4**, 3826.

S7 S. M. Atakishiev, D. Sh. Abdinov and G. A. Akhundov, *Phys. stat. sol. (b)*, 1968, **28**, K47–K50.